Biosensors and Bioelectronics ■ (■■■■) ■■■–■■■

Contents lists available at ScienceDirect

Biosensors and Bioelectronics

journal homepage: www.elsevier.com/locate/bios

A high sensitivity field effect transistor biosensor for methylene blue detection utilize graphene oxide nanoribbon

Ting-Chun Lin [a], Yan-Sheng Li [b], Wei-Hung Chiang [b], Zingway Pei [a,c,*]

[a] Department of Electrical Engineering, National Chung Hsing University, Taichung 40227, Taiwan
[b] Department of Chemical Engineering, National Taiwan University of Science and Technology, Taipei 10607, Taiwan
[c] Graduate Institute of Optoelectronic Engineering, National Chung Hsing University, Taichung 40227, Taiwan

ARTICLE INFO

Article history:
Received 29 December 2015
Received in revised form
20 February 2016
Accepted 17 March 2016

Keywords:
Graphene oxide nanoribbon
Methylene blue
Field effect transistor
Sensitivity

ABSTRACT

In this work, we developed a field effect transistor (FET) biosensor utilizing solution-processed graphene oxide nanoribbon (GONR) for methylene blue (MB) sensing. MB is a unique material; one of its crucial applications is as a marker in the detection of biomaterials. Therefore, a highly sensitive biosensor with a low detection limit that can be fabricated simply in a noncomplex detection scheme is desirable. GONR is made by unzipping multiwall carbon nanotubes, which can be mass-produced at low temperature. The GONR-FET biosensor demonstrated a sensitivity of 12.5 μA/mM (determined according to the drain current difference caused by the MB concentration change). The Raman spectra indicate that the materials quality of the GONR and the domain size for the C=C sp^2 bonding were both improved after MB detection. X-ray photoelectron spectroscopy revealed that the hydroxyl groups on the GONR were removed by the reductive MB. According to XPS and Raman, the positive charge is proposed to transfer from MB to GONR during sensing. This transfer causes charge in-neutrality in the GONR which is compensated by releasing •OH functional groups. With high sensitivity, a low detection limit, and a simple device structure, the GONR-FET sensor is suitable for sensing biomaterials.

1. Introduction

Methylene blue (MB) is a crucial chemical that has wide-ranging applications. It is used in analytical chemistry as a pH indicator (Deboux et al., 1995); dye for cellulose and bacteria (Wu et al., 2009; Zhou et al., 2014); and agar for bacteria such as *Escherichia coli*, gram-negative bacteria, *Salmonella*, and *Shigella* (Taylor, 1971; Usacheva et al., 2001) as well as a marker for DNA (Liu et al., 2012; Rafiee-Pour et al., 2016) and damaged DNA that lead to cancer (Gruetter et al., 1981; Soni et al., 2009). By detecting the concentration of the MB, the information that including the pH value, the redox level, the DNA's concentration, and the bacteria's growth rate can be obtained under a controlled sensing environment. To design a biosensor, two issues are critical: sensing techniques and sensor materials. For the techniques, both electrical and optical methods are used for detecting MB. For optical detection, the shift in Ag nanoparticles' plasmonic resonance peaks in the presence of MB were recorded to identify the concentration (Luo et al., 2013). By comparing the optical signals for the reference MB with known concentration and the MB with species to be detected, the shift in the spectra could deduce the concentration of the species under test. In addition to plasmonic resonance, the intensity of optical excitation spectra for MB in photoreduction experiments is used to determine the concentration (Kadokawa et al., 2011). Moreover, MB has been used in the capture probe–target–signal probe electrochemical sensing method for *E. coli* detection (Li et al., 2015). Electrically, the cyclic voltammetry and amperometric measurements are used detect horseradish peroxidase by coimmobilized with methylene blue onto a carbon electrode surface. The feasibility of MB as an electron carrier between peroxidase and the carbon electrode were detected (Xu et al., 2003). Square-wave voltammetry utilizes the redox behaviors of MB in the presence of the species being detected (Lovrić and Komorsky-Lovric, 1988; Xu et al., 2003). And the ion-sensitive field effect transistor (ISFET) based on Silicon was used for DNA and biomaterials detection (Lee et al., 2009; Zayats et al., 2006). The ISFET could either conduction current or the threshold voltage shift for bio-detection. Upon the binding of to the cognate aptamer, changes in the electrical signal were monitored with an ISFET. By immobilization of amine-functionalized aptamer on the gate surface, the ISFET is used to sense adenosine in a detection limit of approximately 5×10^{-5} M and showed high specificity. Theoretically, FET based structure detect electrical

* Corresponding author at: Department of Electrical Engineering, National Chung Hsing University, Taichung 40227, Taiwan.
E-mail address: zingway@dragon.nchu.edu.tw (Z. Pei).

http://dx.doi.org/10.1016/j.bios.2016.03.046
0956-5663/

signal caused by the charge transfer which is essentially counted by number of electrons that enabling high sensitivity detection because the instruments used in current detection generally exhibit pA to fA detection ability. On the contrary, the setup for detection small amount of photons is sophisticated and costly. Therefore, the FET based electrical detection probability the better choice for compact, label-free and precise biosensor.

On the other hand, material is a critical issue. Recent development of graphene oxide (GO) may provide a multifunction platform for variety of biomaterial detection for it is possible to decorated surface by carboxyl, hydroxyl, epoxy and other specific functional groups that facilitate specificity (Liu et al., 2010). In their work, the biocompatibility of GO was demonstrated on a cell line derived from human retinal pigment epithelium that exhibit good adhesion and differentiation on the GO film and is visualized after 72 h of culture time. In addition, many biosensors utilize graphene oxide was reported. The graphene oxide was used in an Immunobiosensor for pathogen detection (Jung et al., 2010). Used for bovine albumin serum adsorption in a surface plasmon resonance structure (Chiu and Huang, 2014).The fluorescent of the aptamer-functionalized graphene oxide for mercury(II) detection were also reported (Huang et al., 2014; Li et al., 2013). The GO was blended with chitosan as nanocomposite for typhoid detection (Singh et al., 2013). Recently, the graphene oxide was used to detect the platelet-derived microparticles, which is a major risk factor for arterial pro-thrombotic pathologies (Kailashiya et al., 2015). Since many chemicals and biomaterials are in solution form, and direct measurement in solution is more efficient and useful. In this work, we derived GO from Graphene nanoribbon (GNR). GNR is a unique form of graphene that has spurred intensive interest because of its exceptional electronic property, thermal stability, and low percolation threshold (Han et al., 2007; Li et al., 2008; Son et al., 2006). Recent theoretical and experimental works have demonstrated that GNR is a promising material for numerous applications such as in energy generation and storage (Liu et al., 2014a; Uthaisar and Barone, 2010; Wang 2015), chemicals and biosensors (Hou et al., 2014; Wang et al., 2010), catalysis (Davis et al., 2014; Holby and Taylor, 2012), and nanoelectronics (Fiori and Iannaccone, 2007; Wang et al., 2008). In general, GNR represents a long strip of graphene with width ranging from sub-10 nm to several hundred nanometers while the thickness is about of several nanometers. (Cai et al., 2010; Han et al., 2007; Kosynkin et al., 2009; Ma et al., 2013a; Shimizu et al., 2011). Unlike graphene sheets that feature a zero bandgap, GNR possesses an open bandgap that can be controlled by tuning atomic-scale structures. For example, GNR with designed edges can effectively modulate the electronic energy gap, thus enhancing the charge transfer and chemical reactivity when used for chemical and biological detection. The reduction of graphene oxide nanoribbon (GONR) is a promising alternative for the bulk production of GNR-based materials because it can be synthesized in large quantities (Ma et al., 2013b). (Kosynkin et al., 2009; Shimizu et al., 2011) successfully mass produced GONR through chemical oxidation by longitudinally cutting and unraveling multiwalled carbon nanotubes (MWCNTs) in concentrated sulfuric acid and potassium permanganate. Longitudinally unzipping carbon nanotubes through chemical oxidation with a suitable oxidant should be one of the most effective means of achieving low-cost and scalable GNR synthesis (Ma et al., 2013a). In addition, this method can be used to generate oxygen-containing groups around the GNRs, thus adding solution-processing ability to the GNR process for industry-oriented device preparation (Liu et al., 2014b).

In this work, we utilized an field effect transistor (FET) in a solution as a biosensor in which the FET-based biosensor potentially exhibits high sensitivity and a low detection limit (Lee et al., 2009). GONR was used as the detection materials for its exceptional oxidation level tunable conductivity. Furthermore, the MB was used as the detection target to demonstrate the biomaterial detectability in GONR FET biosensors for its wide application and especially because it is usually used as an indicator/marker for the biomaterials.

2. Experiment

2.1. Chemicals

Potassium permanganate ($KMnO_4$, 98%), hydrogen peroxide (H_2O_2, 35%), and ether [$(C_2H_5)_2O$, 99+%] were purchased from Acros. Potassium nitrate (KNO_3, 95%) and ethylene glycol [$C_2H_4(OH)_2$, 99%] were obtained from JT-Baker. Sulfuric acid (H_2SO_4, >95%) and hydrochloric acid (HCl, 37%) were purchased from Scharlau. N-Butanol (C_4H_9OH, >99%) was purchased from Merck. Methylene blue (3,7-bis(Dimethylamino)phenazathionium chloride, $C_{16}H_{18}ClN_3S \cdot xH_2O$), with high purity and biological stain certification was purchase from Alfa Aesar. All the chemicals were used without any further purification.

2.2. GONR preparation

The CNTs used in the present study were MWCNTs synthesized through water-assisted catalytic chemical vapor deposition. The CNT growth process and GONR preparation were similar to those previously described (Chiang et al., 2011; Chiang et al., 2015; Wang, 2015). In a typical preparation of GONR, 0.1 g of MWCNTs was suspended in 10 mL of concentrated H_2SO_4 and 1 g of KNO_3 and was then stirred at 300 rpm for 2 h by using a magnetic stirrer until a visually homogeneous black solution formed. Subsequently, 0.5 g of $KMnO_4$ was slowly added to the solution and further stirred for 2 h at room temperature. The temperature was then gradually increased to 70 °C and maintained at that temperature in a water bath for 2 h (IKA-HS7 digital). When the reaction was complete, the mixtures were removed from the heat source, allowed to cool to room temperature, and poured into 350 g of ice containing 5 mL of 35% H_2O_2 each to prevent precipitation of insoluble MnO_2. The mixtures were then centrifuged (24,500 rpm, 30 min) to make the crude GNRs solid (Beckman, Avanti J-25). The solid was removed and then bath-sonicated in 60 mL of deionized (DI) water for 30 min (IKA-HS7 digital). The material was bath-sonicated again by adding 30 mL of HCl, and then the dispersion was centrifuged (24,500 rpm, 30 min). The collected solid was removed and then bath-sonicated in 60 mL of ether for 30 min. Finally, the purified GONRs were obtained by collecting the centrifuged (24,500 rpm, 30 min) solid. The collected solid was oven-dried at 70 °C for 24 h to yield the final GONR product.

2.3. Material characterizations

The SEM images were produced on JEOL JSM-6500F (accelerating voltage=15 kV). Samples were prepared by pressing as-synthesized samples on copper tape. The TEM images were collected using a Hitachi H-9500 transmission electron microscope. Additional samples were prepared by dispersing as-synthesized samples in ethanol and dropping them onto 300 mesh holey lacy carbon grids on a copper support (Ted Pella, Inc.) under ambient conditions. Raman spectra were obtained using a JASCO NRS-5100 at 532-nm excitation and a Tokyo Instruments Nanofinder 30 at 488-nm excitation. X-ray photoelectron spectroscopy (XPS) spectra were obtained using a ULVAC-PHI PHI 5000 Versaprobe with a microfocused raster-scanned X-ray beam induced by high-energy electrons impinging on Al anodes.

Please cite this article as: Lin, T.-C., et al., Biosensors and Bioelectronics (2016), http://dx.doi.org/10.1016/j.bios.2016.03.046

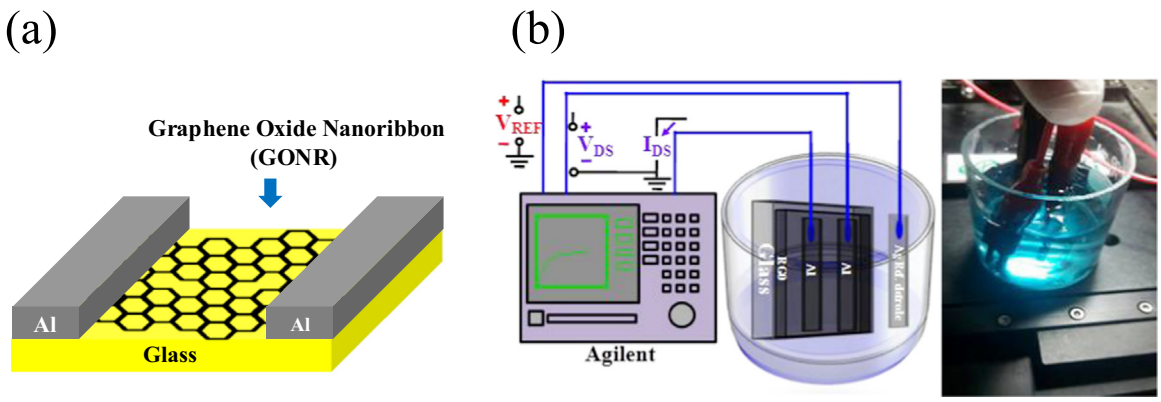

Fig. 1. (a) Device structure and (b) sensing scheme of the GONR-FET biosensor.

2.4. GONR FET biosensor preparation

The GONRs obtained by unzipping MWCNTs were dissolved in 1:1 mixed n-butanol and water at 0.001 wt% as the precursor. After being fully stirred, the GONR solution was spin-coated on a glass substrate. The spinning was conducted in two stages. The first stage was performed at 400 rpm for 5 s to promote uniform GONR distribution on the glass. The second step was performed at 800 rpm for 30 s to yield a relatively thin GONR layer and to evaporate the solvent. After natural drying, some GONR samples were placed on a hotplate at 200 °C for 30 min. This thermal treatment could break some of the hydroxyl bonds attached to the GONR to form slightly reduced GONR. After thermal reduction, a 100-nm-thick Al was deposited on the GONR and rGONR through a shadow mask as the source and drain electrodes. The device structure for the GONR FET biosensor is depicted in Fig. 1(a).

2.5. MB measurements

The GNOR FET biosensors were then placed in the MB solution for measurement. Since the molecular weight for MB is 319.85 g mol^{-1}, 9.5955 g of MB was dissolved in the 100 mL deionizd (DI) water to prepare MB solution in 0.3 M. This solution was further dilute by DI water to prepare other concentrations. The concentrations of the MB varied from 0.4 to 0.3 M were used. An Ag rod was used as the reference electrode. Before measurement, the Ag rod was immersed in the HCl to produce a stable AgCl electrode. An Agilent B2912 source-meter semiconductor parameter analyzer was connected to the AgCl and source/drain electrodes to obtain electrical measurements. The schematic diagram and the photo picture for the GONR FET biosensor measurement setup is shown in Fig. 1(b).

3. Results and discussion

3.1. GONR characterization

The morphologies of as-produced GONR were characterized by electronic microscope. Fig. 2(a) shows the SEM image of as-produced product with a ribbon-like morphology due to the CNT unzipping. In addition, the TEM image shown in Fig. 2(b) further verifies the ribbon-like structure with width in the range of several hundred nanometers. Furthermore, the nearly transparent layer structure revealed by the TEM observation indicates the presence of few atomic layers with thickness in the range of several nanometers existed in the as-produced product. The above electronic microscopic study suggests nanoribbon structure was produced in our as-produced sample, which is in consistent with previous reports (Kosynkin et al., 2009; Shimizu et al., 2011). Further structural information of the as-produced GONR can be obtained from micro Raman spectroscopy characterization. Fig. 2 (d) shows the representative Raman spectra of the pristine CNTs and as-produced GONR. Three bands are present around 1320 cm^{-1}, 1590 cm^{-1}, and 2675 cm^{-1}, which are respectively assigned to the D, G, and 2D bands of carbon materials. The D band

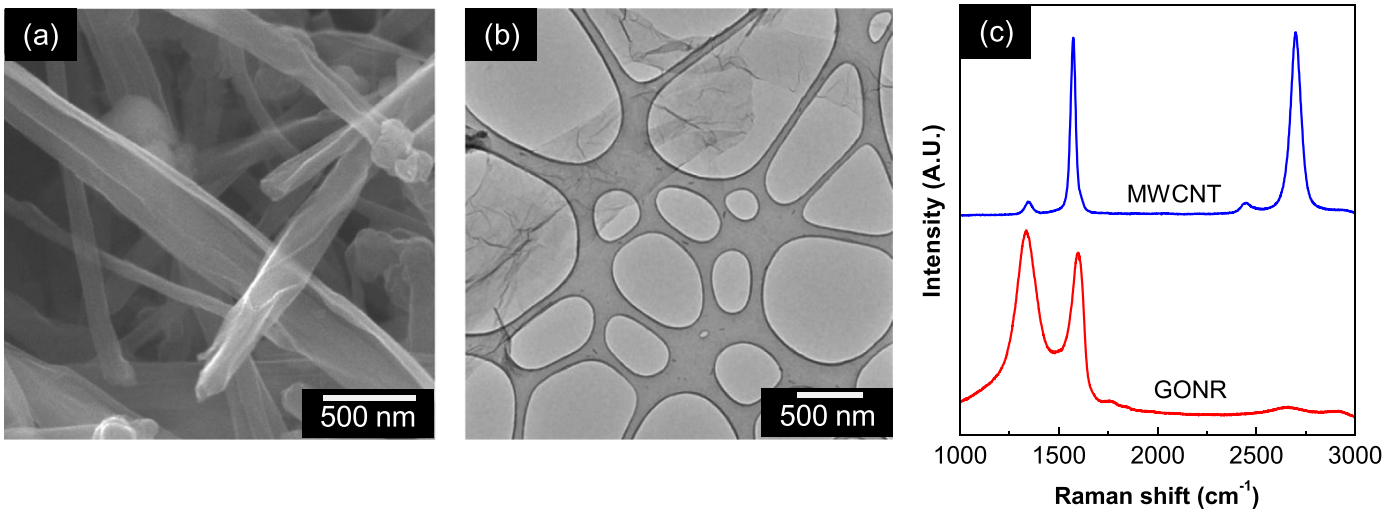

Fig. 2. (a) SEM and (b) TEM images of as-produced GONR. and (c) Raman spectra of starting MWCNT (blue lines) and as-produced GONR (red lines). (For interpretation of the references to color in this figure legend, the reader is referred to the web version of this article)

Please cite this article as: Lin, T.-C., et al., Biosensors and Bioelectronics (2016), http://dx.doi.org/10.1016/j.bios.2016.03.046

can be due to the structural imperfections in the carbon basal plane or edge site (Ferrari and Robertson, 2000; Malard et al., 2009), whereas the G band is the so-called characteristic peak of graphite, corresponding to the sp^2 carbon bond stretching of E2g mode (Malard et al.,, 2009). The 2D band is the overtone of the D band and is typically used to indicate graphene structure quality (Ferrari et al., 2006; Graf et al., 2007). After the oxidative unzipping process, the intensity of the D and 2D bands increased and decreased, respectively, indicating that defects or the edge effect was introduced into the as-produced GONR. The defects could have been holes with different shapes and sizes on the basal plane of the ribbon caused by the initial manganate ester formation and the further cleavage of C–C bonding introduced by the vicinal diols (Higginbotham et al., 2010). Moreover, the attached oxygen functional groups (i.e., epoxy, carbonyl, and carboxyl groups) at the edges and surface were also regarded as defects (Higginbotham et al., 2010). Overall, these characterizations suggest that the GONR was successfully prepared using our method.

3.2. Current–voltage characteristics

The drain current-voltage characteristics of the GONR and rGONR FET biosensors are displayed in Fig. 3(a). During the measurement, the source electrode is grounded. And the drain-to-source voltage is swept from 0 to 10 V, while the reference voltage was kept at 10 V. The drain current of the GONR and rGONR FET biosensors at 5 V are around 7.3×10^{-8} A and 6.2×10^{-4} A, respectively. The reduction by thermal annealing at 200 °C enhances the drain current by 4 orders of magnitude. They are used as the reference current for MB detection. The MB with a concentration of 0.025 to 0.3 M were measured by rGONR FET biosensors. The drain current increased with the MB concentration. At 5 V, the drain of the rGONR FET biosensor under ambient conditions was 6.2×10^{-4} A and increased to 1.1×10^{-3} A under 0.025 M of MB. Furthermore, it is increased to 7.48×10^{-3} A under 0.3 M of MB. The drain current increased more than 10-fold. The current through the reference electrode remained as low as 1×10^{-9} A, indicating a typical FET type biosensor operation. The applied drain voltage also affected the drain current of the rGONR-FET biosensor. The drain current for the rGONR-FET biosensor under 0.3 M of MB increased rapidly from 2.61 to 13.7 mA as the drain voltage increased from 5 μV to 10 V. By contrast, the drain current increased less for the rGONR-FET without MB. This indicates the interaction of MB with rGONR will increase conductivity of the rGONR. And this conductivity enhancement is proportional to the concentration of MB. To detect MB at lower concentration, a GONR as a detection channel in a FET biosensor is expected. As shown in the Fig. (a), the GONR-FET biosensor was used to detect MB at concentration from 0.8 to 3 mM. As a result, the GONR FET biosensor can detect MB at much lower concentration. The drain current is 4.4×10^{-5} A for a GONR-FET to sense 0.8 mM of MB at 5 V drain voltage. Notably, the interaction of the MB and rGONR is irreversible. After the sensing of 0.3 M of MB, the drain current of the rGONR-FET biosensor was measured again under air and DI water. The current–voltage characteristics are shown in Fig. 3(b). The three curves almost coinciding indicate a possible electrochemical interaction between the MB and rGONR. A similar effect was previously found in CNT, in which the MB was positively charged and interacted with CNT through charge transfer to form an electrochemically functional MB–CNT nanostructure (Yan et al., 2005). This effect may have been applied to the MB sensing by the GONR. In this work, the charge transfer may cause the GONR reduced chemically thereby increasing the conductivity of the GONR. And, this conductivity increasing is expected to last for a long time. They are invariant either in the air or in the DI water.

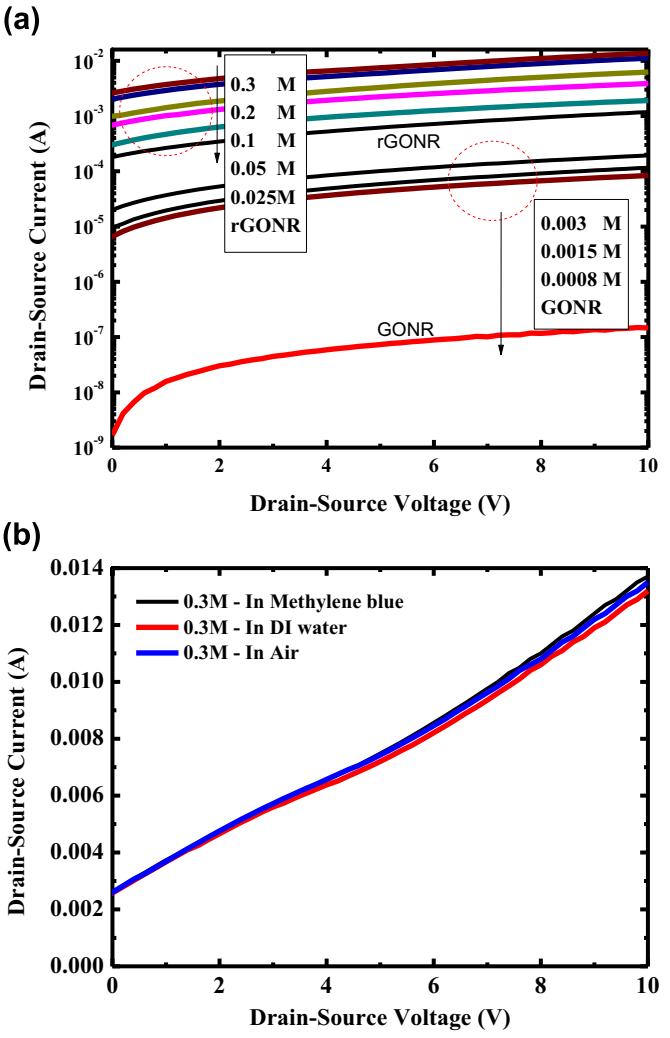

Fig. 3. (a) The drain current–voltage output characteristics for the rGONR- and GONR- FET biosensor. The concentration of methylene blue (MB) is varied from 0.025–0.3 M was used for detection in a rGONR FET. And the concentration of MB is varied from 0.8 to 3 mM for detection in a rGONR FET. (b) The drain current-voltage output characteristics for rGONR FET biosensor that immersed in 0.3 M of MB, immersed in the DI water and blow-dry and measured in the air, respectively. The drain sensing current is invaried.

3.3. Sensor sensitivity

The sensitivity of the rGONR and GONR FET biosensors are determined by the ratio of current change to concentration change in the MB. The drain current at 5 μV, 3 V, and 5 V drain voltage regarding MB concentration is shown in Fig. 4(a) and (b) for rGONR FET and GONR FET, respectively. The calculated sensitivity for the rGONR FET at 5-μV, 3-V, and 5-V drain voltage was 7.8, 16.5, and 28.9 μA/mM, respectively. With lower concentration of MB on GONR-FET, the sensitivity is slightly reduced. The calculated sensitivity for GONR FET at 5-μV, 3-V, and 5-V drain voltage was 2.7, 7.8, and 12.5 μA/mM, respectively. The possible detection limit for this FET biosensor can be extrapolated by the line along the sensitivity curve with the signal-to-noise ratio (SNR) of 10. Since the reference drain current of GONR FET biosensor with at 5 V is 7.3×10^{-8} A, we could set 7.3×10^{-8} A as the detection limit. This limit is estimated around 4.7 nM. However, this limit need further confirmation, because biosensor usually follow Langmuir-Hill behavior in which the signal is insensitive to very small amount of

Please cite this article as: Lin, T.-C., et al., Biosensors and Bioelectronics (2016), http://dx.doi.org/10.1016/j.bios.2016.03.046

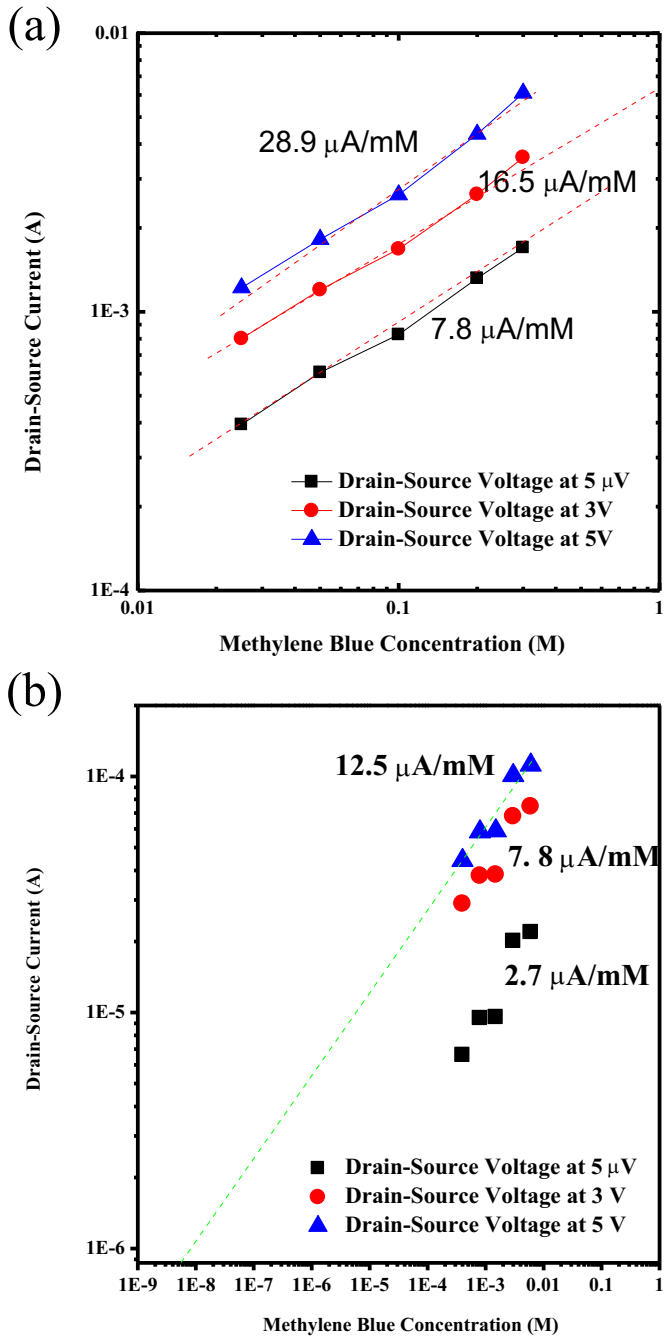

Fig. 4. (a) The semi-logarithm plot of the detection current of a rGONR FET biosensor along with MB concentration for different drain voltage (5 μV, 3 V and 5 V). The sensitivity is calculated as 7.8 μA/mM, 16.5 μA/mM and 28.9 μA/mM, respectively. (b) The logarithm plot of the detection current of a GONR FET biosensor along with MB concentration for different drain voltage (5 μV, 3 V and 5 V). The sensitivity is calculated as 2.7 μA/mM, 7.8 μA/mM and 12.5 μA/mM, respectively. Consider the signal-to-noise (SNR) of 10, the detection limit is estimated by extrapolate plot to as 4.7 nM of MB.

biomaterials. This result is superior to those of other methods. For example, the optical excitation spectrum can detect the 313-μM MB in the photoreduction experiment (Kadokawa et al., 2011). Cyclic voltammetry and amperometric measurements have a detection limit of 1 μM for hydrogen peroxide detection when MB is used as the coimmobilization agent on the CNT electrode (Xu et al., 2003).

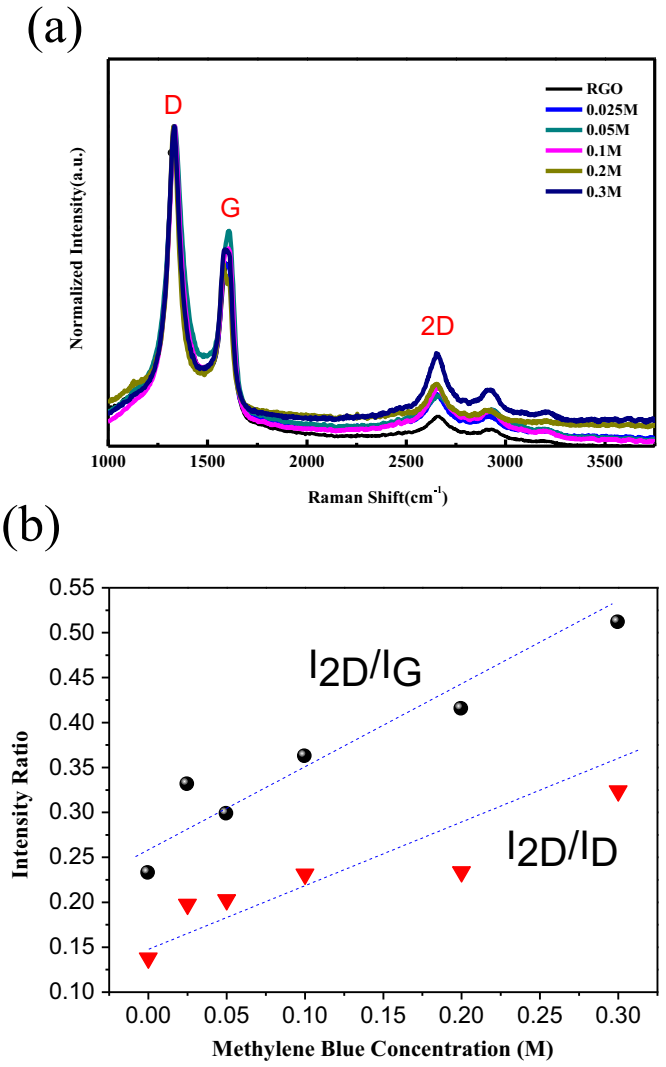

Fig. 5. (a) The Raman spectra and (b) the I_{2D}/I_G and I_{2D}/I_D of the GONR after MB immersion with different concentrations.

3.4. Sensing mechanism

The interaction of the MB to the rGONR was studied through Raman spectroscopy and XPS. The normalized Raman spectroscopy of the rGONR after immersion in the MB sensing with different concentrations is shown in Fig. 5(a). The D (1336 cm^{-1}), G (1592 cm^{-1}), and 2D (2659 cm^{-1}) peaks for the graphene are clearly visible. The extensive D peak is due to structural imperfections caused by the presence of oxygen-related functional groups. The G peak is the characteristic peak of graphite, corresponding to the sp^2 carbon bond-stretching mode. The 2D band is the overtone of the D band and is typically used to indicate graphene film quality, as discussed in Section 3.1. When the D peaks were normalized to unity for all samples, the intensity of the 2D peaks increased gradually with MB concentration. Fig. 5 (b) displays the intensity of the 2D peak to the G peak (I_{2D}/I_G) and of the 2D peak to the D peak (I_{2D}/I_D) in terms of MB concentration. The 2D–G ratio increased from 0.23 for the nontreated rGONR to 0.52 for the rGONR immersed in the 0.3 M MB. The increased I_{2D}–I_G intensity ratio revealed that the quality of the rGONR was improved by the MB. The 2D band was found to be enhanced with respect to the D band, suggesting that the MB treatment increased the sp^2 graphene domain size in the rGONR. According to the layer quality improvement and average rGONR domain size increase

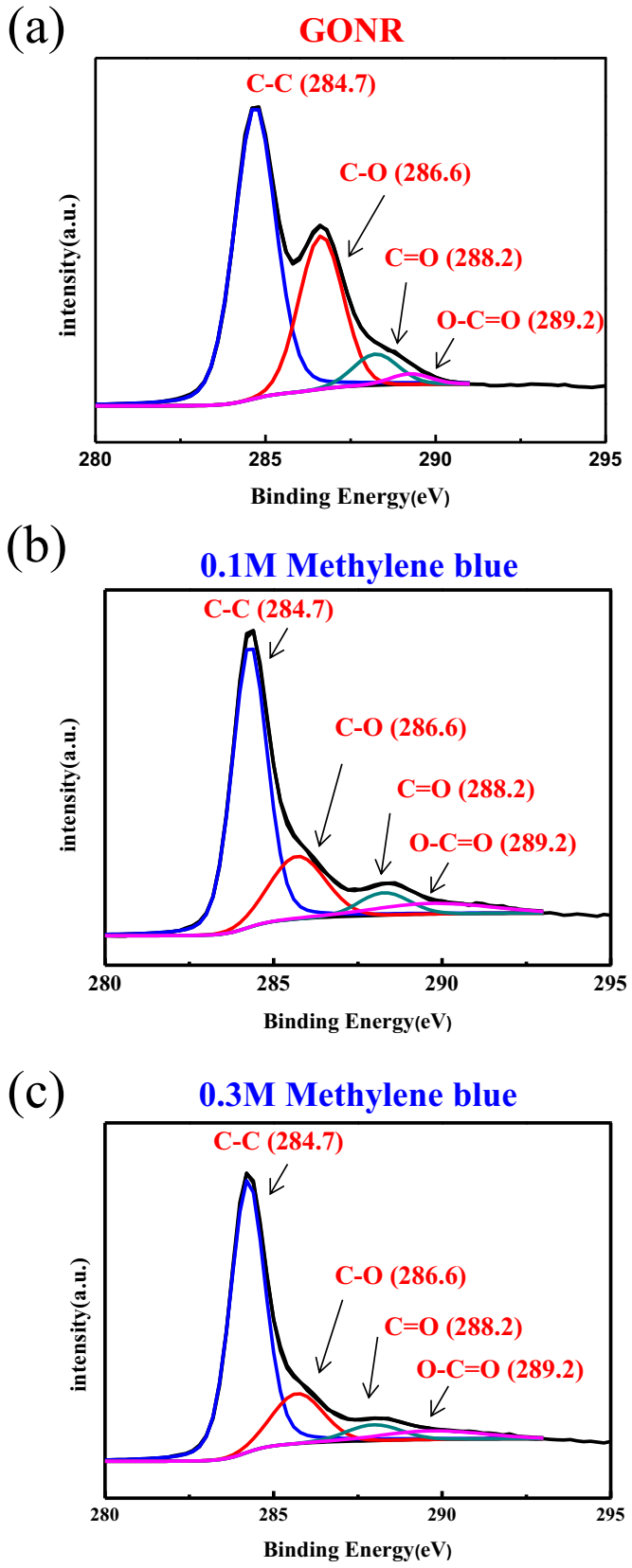

Fig. 6. The XPS C1s peaks for (a) pristine GONR and (b) 0.1 M and (c) 0.3 M MB immersed GONR.

after MB treatment, we might suggest that the MB plays a vital role in the reduction and recovery of the graphene. This suggests that during charge transfer, part of the MB in the solution takes away one type of functional group to further rGONR reduction. To understand which type of the functional group was taken away, XPS was performed on the GONR and GONR immersed in the MB at different concentrations (0.1 and 0.3 M). The C1s peak in the XPS for GONR, GONR with 0.1-M MB treatment, and GONR with 0.3-M MB treatment are shown in Fig. 6(a)–(c), respectively. In the figure, the C1s peak is deconvoluted into C=C, C–O, C=O, and O–C=O bonds. The C–O bond was substantially reduced after MB treatment, indicating that the MB tends to take the hydroxyl (OH^-) group away from GONR. This is revealed by the atomic concentration for each bond listed in Table 1. The GONR had 61.2% of the C–C bond and 28.9% of the C–O bond. The total proportions of the C=O and O–C=O bonds were approximately 10%. After 0.3-M MB treatment, the C–C bond proportion had increased to 71%, whereas the C–O bond proportion had decreased to 17.2%. The total amount of the C=O and O–C=O proportions remained approximately 11.5%. The XPS results revealed a reduction in the oxygen functional groups and an increase in the C–C bond. These results are consistent with our Raman spectrum finding and suggestion that the MB takes the OH^- group away, leaving GONR with an enlarged graphene domain. According to XPS and Raman results, the chemical reaction between MB and GONR and rGONR can be suggested. Methylene blue is a reductive chemical and is positively charged. The positive charge may transfer to the GONR in the solution cause the charge in-neutrality. This in-neutrality may be compensated by releasing •OH groups into the solution. As a consequence, the GONR is reduced. Although this process need to be verified and may contain other possibility, the results of GONR reduction after •OH releasing and the increased in graphene domain by C bond reconstruction is confirmed experimentally.

Table 1
The atomic concentration for C–C, C–O, C=O and O–C=O bondings in the XPS C1s peak of GONR after methylene blue immersion.

Samples	C–C (at%)	C–O (at%)	C=O (at%)	O–C=O (at%)
GONR	61.2	28.6	7.1	3.1
0.1 M MB Treated GONR	64.9	20.8	6.7	7.4
0.3 M MB Treated GONR	71.1	17.2	5.7	5.8

4. Conclusion

Our preliminary work demonstrates a FET type biosensor based on graphene oxide nanoribbon (GONR) for methylene blue detection. The GONRs are obtained by unzipping MWCNTs in acid. By using rGONR FET biosensor, the sensing current as high as 7.48 mA was obtained for 0.3 M of MB detection. Even with 0.8 mM of MB, the sensing current is still as high as 44 μA. As a result, MB has extensive reaction with GONR. By calculation, the highest sensitivity at 5 V is 28.9 μA/mM on rGONR-FET biosensor. With GONR-FET biosensor, the sensitivity reduced to 12.5 μA/mM. The sensing mechanism is attributable to the increase in the conduction of the GONR after immersion in the MB. The Raman spectra for rGONR after MB sensing suggest the structural imperfection of rGONR is improved and the sp^2 graphene domain is enlarged by the enhanced 2D peaks respect to D and G peaks. Furthermore, some of the oxygen-related imperfections, especially hydroxyl groups (•OH), was removed by the MB suggesting by the XPS spectra. According to XPS and Raman, the positive charge is proposed to transfer from MB to GONR during sensing. This transfer causes charge in-neutrality in the GONR which is compensated by releasing •OH functional groups. Overall, the GONR-FET biosensor exhibited high sensitivity and a low detection limit that is highly suitable for detecting low concentrations of biomaterials.

Please cite this article as: Lin, T.-C., et al., Biosensors and Bioelectronics (2016), http://dx.doi.org/10.1016/j.bios.2016.03.046

Acknowledgement

This work is financially supported by Ministry of Science and Technology (MOST), Taiwan under Grant nos. MOST 104-2221-E-005-074-, MOST 103-2221-E-011-150-MY2, and MOST 104-2923-E-011-001-MY3.

References

Cai, J.M., Ruffieux, P., Jaafar, R., Bieri, M., Braun, T., Blankenburg, S., Muoth, M., Seitsonen, A.P., Saleh, M., Feng, X.L., Mullen, K., Fasel, R., 2010. Atomically precise bottom-up fabrication of graphene nanoribbons. Nature 466 (7305), 470–473.

Chiang, W.-H., Futaba, D.N., Yumura, M., Hata, K., 2011. Growth control of single-walled, double-walled, and triple-walled carbon nanotube forests by a priori electrical resistance measurement of catalyst films. Carbon 49 (13), 4368–4375.

Chiang, W.-H., Lin, T.-C., Li, Y.-S., Yang, Y.-J., Pei, Z., 2015. Toward bandgap tunable graphene oxide nanoribbons by plasma-assisted reduction and defect restoration at low temperature. RSC Adv.

Chiu, N.-F., Huang, T.-Y., 2014. Sensitivity and kinetic analysis of graphene oxide-based surface plasmon resonance biosensors. Sens. Actuators B: Chem. 197, 35–42.

Davis, D.J., Raji, A.R.O., Lambert, T.N., Vigil, J.A., Li, L., Nan, K., Tour, J.M., 2014. Silver-graphene nanoribbon composite catalyst for the oxygen reduction reaction in alkaline electrolyte. Electroanalysis 26 (1), 164–170.

Deboux, B.J.C., Lewis, E., Scully, P.J., Edwards, R., 1995. A novel technique for optical fiber pH sensing based on methylene blue adsorption. J. Light. Technol. 13 (7), 1407–1414.

Ferrari, A.C., Robertson, J., 2000. Interpretation of Raman spectra of disordered and amorphous carbon. Phys. Rev. B 61 (20), 14095.

Ferrari, A.C., Meyer, J.C., Scardaci, V., Casiraghi, C., Lazzeri, M., Mauri, F., Piscanec, S., Jiang, D., Novoselov, K.S., Roth, S., 2006. Raman spectrum of graphene and graphene layers. Phys. Rev. Lett. 97 (18), 187401.

Fiori, G., Iannaccone, G., 2007. Simulation of graphene nanoribbon field-effect transistors. Electron Device Lett., IEEE 28 (8), 760–762.

Graf, D., Molitor, F., Ensslin, K., Stampfer, C., Jungen, A., Hierold, C., Wirtz, L., 2007. Spatially resolved Raman spectroscopy of single-and few-layer graphene. Nano Lett. 7 (2), 238–242.

Gruetter, C.A., Gruetter, D.Y., Lyon, J.E., Kadowitz, P.J., Ignarro, L.J., 1981. Relationship between cyclic guanosine 3′:5′-monophosphate formation and relaxation of coronary arterial smooth muscle by glyceryl trinitrate, nitroprusside, nitrite and nitric oxide: effects of methylene blue and methemoglobin. J. Pharmacol. Exp. Ther. 219 (1), 181–186.

Han, M.Y., Özyilmaz, B., Zhang, Y., Kim, P., 2007. Energy band-gap engineering of graphene nanoribbons. Phys. Rev. Lett. 98 (20), 206805.

Higginbotham, A.L., Kosynkin, D.V., Sinitskii, A., Sun, Z., Tour, J.M., 2010. Lower-defect graphene oxide nanoribbons from multiwalled. Carbon Nanotub. ACS Nano 4 (4), 2059–2069.

Holby, E.F., Taylor, C.D., 2012. Control of graphene nanoribbon vacancies by Fe and N dopants: implications for catalysis. Appl. Phys. Lett. 101 (6), 064102.

Hou, Y., Li, J., Wen, Z., Cui, S., Yuan, C., Chen, J., 2014. N-doped graphene/porous g-C3N4 nanosheets supported layered-MoS2 hybrid as robust anode materials for lithium-ion batteries. Nano Energy 8, 157–164.

Huang, J., Gao, X., Jia, J., Kim, J.-K., Li, Z., 2014. Graphene oxide-based amplified fluorescent biosensor for Hg2+detection through hybridization chain reactions. Anal. Chem. 86 (6), 3209–3215.

Jung, J.H., Cheon, D.S., Liu, F., Lee, K.B., Seo, T.S., 2010. A graphene oxide based immuno-biosensor for pathogen detection. Angew. Chem. 49 (33), 5708–5711.

Kadokawa, J.-i, Izawa, H., Ohta, T., Wakizono, S., Yamamoto, K., 2011. Photo-induced reduction reaction of methylene blue in an ionic liquid. Int. J. Org. Chem. 01 (04), 158–161.

Kailashiya, J., Singh, N., Singh, S.K., Agrawal, V., Dash, D., 2015. Graphene oxide-based biosensor for detection of platelet-derived microparticles: a potential tool for thrombus risk identification. Biosens. Bioelectron. 65, 274–280.

Kosynkin, D.V., Higginbotham, A.L., Sinitskii, A., Lomeda, J.R., Dimiev, A., Price, B.K., Tour, J.M., 2009. Longitudinal unzipping of carbon nanotubes to form graphene nanoribbons. Nature 458 (7240), 872–876.

Lee, C.S., Kim, S.K., Kim, M., 2009. Ion-sensitive field-effect transistor for biological sensing. Sensors 9 (9), 7111–7131.

Li, F., Yu, Z., Qu, H., Zhang, G., Yan, H., Liu, X., He, X., 2015. A highly sensitive and specific electrochemical sensing method for robust detection of *Escherichia coli* lac Z gene sequence. Biosens. Bioelectron. 68, 78–82.

Li, M., Zhou, X., Ding, W., Guo, S., Wu, N., 2013. Fluorescent aptamer-functionalized graphene oxide biosensor for label-free detection of mercury(II). Biosens. Bioelectron. 41, 889–893.

Li, X., Wang, X., Zhang, L., Lee, S., Dai, H., 2008. Chemically derived, ultrasmooth graphene nanoribbon semiconductors. Science 319 (5867), 1229–1232.

Liu, J., Durstock, M., Dai, L., 2014a. Graphene oxide derivatives as hole- and electron-extraction layers for high-performance polymer solar cells. Energy Environ. Sci. 7 (4), 1297–1306.

Liu, J., Kim, G.H., Xue, Y., Kim, J.Y., Baek, J.B., Durstock, M., Dai, L., 2014b. Graphene oxide nanoribbon as hole extraction layer to enhance efficiency and stability of polymer solar cells. Adv. Mater. 26 (5), 786–790.

Liu, M., Luo, C., Peng, H., 2012. Electrochemical DNA sensor based on methylene blue functionalized polythiophene as a hybridization indicator. Talanta 88, 216–221.

Liu, Y., Yu, D., Zeng, C., Miao, Z., Dai, L., 2010. Biocompatible graphene oxide-based glucose biosensors. Langmuir : ACS J. Surf. Colloids 26 (9), 6158–6160.

Lovrić, M., Komorsky-Lovric, Š., 1988. Square-wave voltammetry of an adsorbed reactant. J. Electroanal. Chem. Interfacial Electrochem. 248 (2), 239–253.

Luo, J., Yao, J., Lu, Y., Ma, W., Zhuang, X., 2013. A silver nanoparticle-modified evanescent field optical fiber sensor for methylene blue detection. Sensors 13 (3), 3986–3997.

Ma, L., Wang, J., Ding, F., 2013a. Recent progress and challenges in graphene nanoribbon synthesis. ChemPhysChem 14 (1), 47–54.

Ma, L., Wang, J.L., Ding, F., 2013b. Recent progress and challenges in graphene nanoribbon synthesis. Chemphyschem 14 (1), 47–54.

Malard, L.M., Pimenta, M.A., Dresselhaus, G., Dresselhaus, M.S., 2009. Raman spectroscopy in graphene. Phys. Rep. 473 (5), 51–87.

Rafiee-Pour, H.A., Behpour, M., Keshavarz, M., 2016. A novel label-free electrochemical miRNA biosensor using methylene blue as redox indicator: application to breast cancer biomarker miRNA-21. Biosens. Bioelectron. 77, 202–207.

Shimizu, T., Haruyama, J., Marcano, D., Kosinkin, D., Tour, J., Hirose, K., Suenaga, K., 2011. Large intrinsic energy bandgaps in annealed nanotube-derived graphene nanoribbons. Nat. Nanotechnol. 6 (1), 45–50.

Singh, A., Sinsinbar, G., Choudhary, M., Kumar, V., Pasricha, R., Verma, H.N., Singh, S. P., Arora, K., 2013. Graphene oxide-chitosan nanocomposite based electrochemical DNA biosensor for detection of typhoid. Sens. Actuators B: Chem. 185, 675–684.

Son, Y.-W., Cohen, M.L., Louie, S.G., 2006. Half-metallic graphene nanoribbons. Nature 444 (7117), 347–349.

Soni, M., Saha, S., Korant, A., Fritz, P., Chakravarty, B., Sirop, S., Gayar, A., Iddings, D., Wiese, D., 2009. A prospective trial comparing 1% lymphazurin vs 1% methylene blue in sentinel lymph node mapping of gastrointestinal tumors. Ann. Surg. Oncol. 16 (8), 2224–2230.

Taylor, W.I., Schelhart., D., 1971. Comparison of xylose lysine deoxycholate agar, Hektoen enteric agar, Salmonella-Shigella agar, and eosin methylene blue agar with stool specimens. Appl. Microbiol. 21, 32–37.

Usacheva, M.N., Teichert, M.C., Biel, M.A., 2001. Comparison of the methylene blue and toluidine blue photobactericidal efficacy against gram-positive and gram-negative microorganisms. Lasers Surg. Med. 29 (2), 165–173.

Uthaisar, C., Barone, V., 2010. Edge effects on the characteristics of Li diffusion in graphene. Nano Lett. 10 (8), 2838–2842.

Wang, C., Li, Y.S., Jiang, J.J., Chiang, W.H., 2015. Controllable tailoring graphene nanoribbons with tunable surface functionalities: an effective strategy toward high-performance lithium-ion batteries. ACS Appl. Mater. Interfaces 7 (31), 17441–17449.

Wang, X., Ouyang, Y., Li, X., Wang, H., Guo, J., Dai, H., 2008. Room-temperature all-semiconducting sub-10-nm graphene nanoribbon field-effect transistors. Phys. Rev. Lett. 100 (20), 206803.

Wang, Y., Shao, Y., Matson, D.W., Li, J., Lin, Y., 2010. Nitrogen-doped graphene and its application in electrochemical biosensing. ACS Nano 4 (4), 1790–1798.

Wu, J., Xu, H., Tang, W., Kopelman, R., Philbert, M.A., Xi, C., 2009. Eradication of bacteria in suspension and biofilms using methylene blue-loaded dynamic nanoplatforms. Antimicrob. Agents Chemother. 53 (7), 3042–3048.

Xu, J.-Z., Zhu, J.-J., Wu, Q., Hu, Z., Chen, H.-Y., 2003. An amperometric biosensor based on the coimmobilization of horseradish peroxidase and methylene blue on a carbon nanotubes modified electrode. Electroanalysis 15 (3), 219–224.

Yan, Y., Zhang, M., Gong, K., Su, L., Guo, Z., Mao, L., 2005. Adsorption of methylene blue dye onto carbon nanotubes: a route to an electrochemically functional nanostructure and its layer-by-layer assembled nanocomposite. Chem. Mater. 17 (13), 3457–3463.

Zayats, M., Huang, Y., Gill, R., Ma, C.A., Willner, I., 2006. Label-free and reagentless aptamer-based sensors for small molecules. J. Am. Chem. Soc. 128 (42), 13666–13667.

Zhou, C., Wu, Q., Lei, T., Negulescu, I.I., 2014. Adsorption kinetic and equilibrium studies for methylene blue dye by partially hydrolyzed polyacrylamide/cellulose nanocrystal nanocomposite hydrogels. Chem. Eng. J. 251, 17–24.

Please cite this article as: Lin, T.-C., et al., Biosensors and Bioelectronics (2016), http://dx.doi.org/10.1016/j.bios.2016.03.046